Experimental investigation of the matching boundary and optimization strategy of a variable geometry turbocharged direct-injected hydrogen engine

Feng-yu Lai [a], Bai-gang Sun [a, b], Shi-wei Zhang [a], Kang-da Wang [a], Qing-he Luo [a, b], Ling-zhi Bao [a,c *], Felix Leach [c]

a School of Mechanical Engineering, Beijing Institute of Technology, Beijing 100081, China

b Beijing Institute of Technology Chongqing Innovation Center, Chongqing, 401121, China

c Department of Engineering Science, University of the Oxford, Oxford, OX1 3PJ, UK

Corresponding: Ling-zhi Bao (Email: paul.bao@eng.ox.ac.uk)

Abstract

With the higher demand for torque, power, brake thermal efficiency (BTE), and low NOx emissions of hydrogen engines, direct injection and turbocharging are the most effective methods to improve performance. However, due to the large air flow rate variation range with lean combustion and low exhaust gas energy, the turbine needs to be adjusted significantly, and the performance of the conventional waste gate turbochargers is limited. In this study, A 2.0 L direct-injected turbocharged hydrogen engine was studied experimentally and matched with a variable geometry turbocharger (VGT). The working boundary of the VGT determined by abnormal combustion and exhaust back pressure is proposed at all working conditions as it changes from 10-50% @1500 rpm to 40-75% @4500 rpm. Control of the VGT to balance combustion and gas exchange was achieved to reach the highest BTE of 42.57%. Further, high torque of 326.6 Nm and high power of 124.2 kW are explored and different VGT opening strategies are compared. An optimized VGT opening control strategy is proposed, which is divided into five phases at different loads to ensure best performance. The VGT opening control strategy based on λ control and the trade-off between combustion and gas exchange efficiency at all working conditions can be valuable in the development of high-performance hydrogen

engines.

Keywords: Hydrogen engine; Direct injection; Variable geometry turbocharger; Controlling strategy

Nomenclature：

PFI	port fuel injected
DI	direct-injected
VVT	variable valve timing
VGT	variable geometry turbine
H_2ICE	Hydrogen internal combustion engine
FGT	fixed geometry turbine
WGT	wastegate turbocharger
IVO	intake valve opening
EVC	exhaust valve closing
λ	excess air ratio
BMEP	brake mean effective pressure
BTE	brake thermal efficiency
IMEP	indicated mean effective pressure
ITE	indicated thermal efficiency
MBT	minimum spark advance for best torque
PEMP	pumping effective mean pressure
PEMP/IMEP	pumping loss ratio
BD	burn duration

Introduction

In order to deal with the damage from the greenhouse effect and environmental pollution, the use of renewable energy is studied worldwide [1], including energy vectors such as hydrogen [2,3], ammonia [4,5], and methanol [6,7]. Hydrogen is a more attractive subject for energy research because of its unique physical and chemical properties, such as zero carbon emissions, a high specific energy content, and a large octane number [8]. As a clean energy carrier, hydrogen is expected to play a major role in energy systems and decarbonization in the future [3,9].

Hydrogen, as an energy carrier, offers the possibility to be used in internal combustion engines [10] and in fuel cells [11]. It is important to mention that these two technologies are complementary rather than competing [12]. Comparing the efficiency of a hydrogen engine with a fuel cell at a similar power class, the superiority of the fuel cell across a wide operating range can be observed, particularly in the low load range. However, at higher loads, the efficiencies of the hydrogen engine and the fuel cell converge. Nevertheless, the greatest advantage of hydrogen engines is their low cost of production, longer service life, and no special requirements for the purity of hydrogen (which is important for a fuel cell). Hydrogen engines even have multi-fuel adaptability and high overall efficiency in high-load areas [8]. In addition, hydrogen has various advantages when it serves as fuel in internal combustion engines, such as a wide ignition range, fast burning velocity, high thermal efficiency, etc. [13,14].

Nevertheless, the hydrogen engine has shown low power output compared to the gasoline engine due to the lower volumetric energy density of hydrogen. With the higher demand for hydrogen engine power performance today, more techniques should be adopted to improve their output power. Although researchers have proposed some mixing-controlled combustion strategies to reduce abnormal combustion, with a lower excess air ratio (λ) to increase the hydrogen engine power density [15], combustion with a low λ leads to other disadvantages. Sterlepper et al. [16] pointed out that lower λ operation leads to higher NOx emissions.

Thus, turbocharging is still a primary method to improve the power output of hydrogen engines. In addition, lean burn (high λ) is useful for hydrogen engines in order to reduce NOx emissions. A large air flow rate is required in hydrogen engines to achieve a lean burn state (defined as λ higher than 2), which is a challenging requirement for hydrogen engine turbocharging.

Various research has shown the potential of turbocharging as an economic and effective method to improve output power. Ford [17] reviewed the development process of a 6.8 L supercharged V-10 Hydrogen internal combustion engine (H_2ICE) and the results showed that the power performance was comparable to or better than that of target gasoline engines. BMW [18] tested a single-cylinder port fuel injected (PFI) H_2ICE with a turbocharger and the specific power is increased by 30% compared with a naturally aspirated gasoline engine. Bosch and TU Graz [8] showed that a specific power of 83 kW/L is achievable with two separate turbochargers acting in the low and the high engine speed ranges. The study of Krishnanunni et al. [19] indicated that the torque of a 4-cylinder 2.5 L turbocharged hydrogen engine can be increased by 140% compared with a naturally aspirated engine. However, the turbocharger could not generate enough boost pressure at low speeds. Bao et al. [20] reported that the power of a turbocharged DI hydrogen engine increased by 123%, and the torque increased by 195% compared to a naturally aspirated engine. The maximum power and torque were attained at 120 kW and 340 Nm respectively. In addition, the maximum power with near-zero emission reached 73 kW at 3000 rpm with well-matched turbocharging [21].

In terms of turbocharging matching for hydrogen engines, Luo et al. [22] showed that poor turbocharger matching of a 2.3 L PFI hydrogen engine leads to a low output power of only about 50 kW, while the maximum power of the gasoline engine reaches about 160 kW. The research of Sterlepper et al. [16] showed that hydrogen engine air flow is limited by the unchanged turbocharging system that comes from the original gasoline engine at high loads when the brake mean effective pressure (BMEP) exceeds 2 MPa. Lee et al. [23]

noted that the back pressure of a turbocharged 2.4 L H_2ICE reaches 0.231 MPa while the intake pressure is only 0.132 MPa at 6000 rpm. In addition, the torque of 84 Nm is lower than that of 98 Nm reached with a naturally aspirated engine. Previous studies have demonstrated that conventional wastegate turbochargers (WGT) of gasoline and diesel engines are limited, especially with large ranges of engine speed and load. Firstly, conventional turbochargers for gasoline engines cannot sustain the energy necessary to provide the required boost pressure because of low exhaust temperatures due to lean burn at low engine speeds in H_2ICE [24]. Furthermore, high back pressures and pumping losses with conventional turbochargers restrict the increase of hydrogen engine power output, especially at high engine speeds [25].

Compared to a WGT, a variable geometry turbine (VGT) is better suited for hydrogen engines because of its wide flow range and high turbine efficiency. The turbocharger can provide sufficient boost pressure by accurately pivoting the angle of the swing blade or by moving the nozzle sidewall [26] to adapt to various exhaust flow rates and temperatures. Previous studies have affirmed the advantages of VGT utilization in diesel and gasoline engines. The research of Wang et al. [27] shows the adaptability of a VGT turbocharger for a 1.85 L light-duty diesel engine at different altitudes. The review of Tang et al. [28] demonstrated that the full-load fuel consumption is improved by 15% with a VGT turbocharger compared with the WGT. The VGT provides better transient response and engine performance [26,29,30], especially at low engine speeds. In addition, the VGT turbocharger operates across a broader operating range and plays an important role in the engine downsizing and emissions improvement process [28,31].

However, the VGT control targets and limits of gasoline engines is mainly focused on exhaust temperature [32,33]; however, in H_2ICE λ control is the priority [34]. The exhaust temperature limit of a VGT in gasoline engines is barely achievable in hydrogen engines which have an exhaust temperature of less than 600 °C. In addition, exhaust back pressure also affects hydrogen engine performance, and the exhaust

back pressure can be adjusted by VGT opening. According to Hiyama et al. [35], a 5.1 L PFI hydrogen engine reaches 2 MPa BMEP and 103% of the low-speed torque of the base diesel engine. The combined 2-stage turbocharging system containing a VGT and a conventional turbocharger is used due to the turbocharging requirements at a wide range of engine speeds. The numerical research of Brin et al. [36] on a 13 L hydrogen engine illustrated the importance of high λ which is set at 2.4 to significantly reduce NOx emissions even at the cost of a poor transient response from the conventional turbocharger. However, the results showed that the selected baseline VGT has high NOx emissions and a slow transient response which can be improved with an E-booster. Kim et al. [37] showed that incorrect turbocharger matching leads to low specific power (lower than 30 kW/L). Their numerical simulation results showed a 1.6 L turbocharged PFI hydrogen engine requires 50% higher mass flow and 90% higher boost pressure compared with gasoline engines, and the high air flow rate is achieved with a VGT. The operating line on the compressor map demonstrated that the demanded boost pressure below 3000 rpm is not achievable with a stock compressor due to surge. The pressure and mass flow demand is mainly influenced by the λ and target performance. The thermodynamic model research from Barış et al. [38] indicated the highest brake thermal efficiency of around 43% is reached with a VGT turbocharger and the FGT turbocharger has the lowest BTE due to low pumping mean effective pressure (PMEP). In addition, the 2-stage turbocharger has a better high-altitude performance compared with a VGT due to a greater margin on the compressor outlet temperature and speed limit. Kim et al. [39] reported the power output of a 2.0 L hydrogen engine with a VGT-type turbocharger increases by 165% compared with naturally aspirated, and the maximum output achieved 84.6 kW at 5000 rpm. On the other hand, the thermal efficiency of a WGT-type turbocharger is similar to the naturally aspirated one due to the pumping loss at high speeds.

In summary, the majority of previous studies are mainly focused on heavy-duty hydrogen engines with

limited speed variation ranges and most of the research is based on numerical simulation. In addition, only some specific working conditions are investigated and there is still a lack of research on the working boundary and controlling strategy of a VGT. In this research, a 2.0 L direct-injected turbocharged hydrogen engine with a VGT was studied at different speeds and loads experimentally. The upper and lower limits of VGT opening at different speeds are presented according to the λ and exhaust back pressure impact. In addition, an optimal VGT control strategy is proposed and balancing effects of pumping loss and λ are discussed to achieve high efficiency. The combined control of VVT and VGT opening is studied, and it is noted that VVT settings should be changed as a priority due to the higher volumetric efficiency when the hydrogen engine operated at high power. Lastly, the optimal VGT control strategy for the whole operating map is proposed and it is divided into five phases to achieve optimal performance.

2. Materials and Methods

2.1 Experimental test bench

The test engine is a 2.0 L four-cylinder DI turbocharged H_2ICE with a VGT turbocharger, which is selected according to the results of reduced flow rate calculations from A. The compression ratio of the original gasoline engine, which this engine is based on, is 10.2, and it is increased to 12.5 by increasing the height of the pistons. Four Bosch HDEV 6 injectors are used to supply sufficient hydrogen for direct injection. The specifications of the H_2ICE are shown in Table 1. The engine test system and data acquisition system were used to obtain experimental data. The layout of the experiment test and data acquisition systems are shown in Figure 1 (a) and (b).

Table 1 The specifications of the DI H_2ICE

Items	Unit	Values
Number of cylinders		4
Bore	mm	80.5
Stroke	mm	98

Displacement	L	2.0
Number of valves		4
Compress ratio		12.5
Turbocharger type		Variable geometry turbine
Engine tests speed	rpm	1500-4000
Hydrogen injection pressure	MPa	6~12

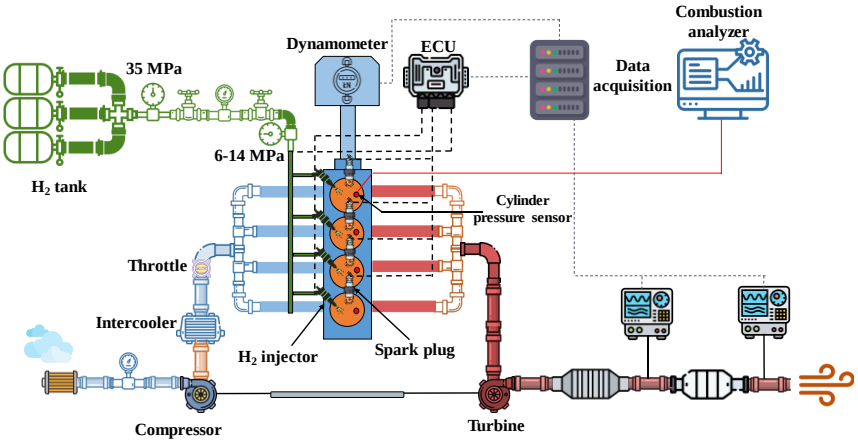

a) Layout of the 2.0 L DI H_2ICE experiment and data acquisition systems

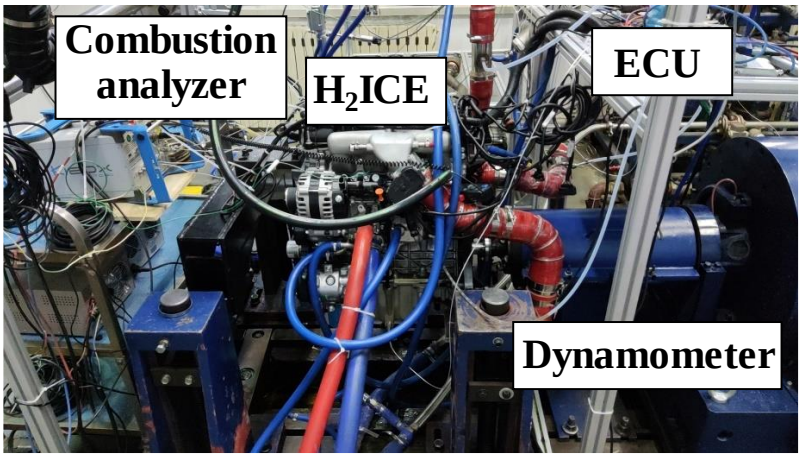

b) Photo of the experimental test rig

Figure 1 The layout of 2.0 L DI H_2ICE and test systems

The test system includes a CW250 eddy current dynamometer, an oil and water temperature controller, air conditioning, and an MTR-500 Air flowmeter. The maximum operating power and speed of the CW250 dynamometer are 250 kW and 8000 rpm respectively. The temperature of the oil and cooling water in the engine is controlled by oil and water temperature controllers. The air mass flow into the engine is measured

with the MTR-500 Air flowmeters and an Emerson CMF010 Coriolis mass flow meter is used to determine the hydrogen mass flow rate. A Kibox combustion analyzer is used in the data acquisition system, and the cylinder pressure is recorded with a Kistler 6052C transducer sensor. The uncertainties of the measured parameters are listed in Table 2. The engine was warmed up before the testing to ensure that the oil and coolant temperatures reached 90°C and 80°C, respectively.

Table 2 The measuring devices and data accuracy

Parameters	Device	Accuracy
Speed	GW250 dynamometer	±1 rpm
Torque	FC2000 Torque transducer	±1 N·m
Pressure	Kistler 6052C transducer	±0.02 MPa
Air mass flow	MTR-500 Air flowmeters	±2.5 kg/h
Hydrogen mass flow	CMF010 H2 flowmeters	±0.01 kg/h
NOx emissions	AVL DiTEST GAS 1000	±3 ppm

Tests were carried out at the minimum spark advance for best torque (MBT) in order to obtain results, and MBT was found by changing the spark timing (ST) at different engine speeds and load conditions. After the H_2ICE operated steadily at the current working condition for two minutes, the average value of the test data from 220 cycles at this operating condition was measured and recorded. The uncertainty of the results was calculated according to the method given by Gürbüz [40], as shown in Equation (1):

$$\Delta R = [\left(\frac{\partial R}{\partial x_1}\Delta x_1\right)^2 + \left(\frac{\partial R}{\partial x_2}\Delta x_2\right)^2 + \cdots \left(\frac{\partial R}{\partial x_n}\Delta x_n\right)^2]^{1/2} \quad (1)$$

where ΔR is the uncertainty in the computed result; R is a given function of the computed results; x_1, x_2, and x_n are the different measured parameters; Δx_1, Δx_2, Δx_n are the corresponding uncertainty of the different measured parameters.

The turbocharger efficiency (TE) in this research is calculated using Equation (2):

$$TE = \frac{\dot{m}_{air} \cdot (C_{p2}T_2 - C_{p1}T_1)}{(\dot{m}_{air} + \dot{m}_{hydrogen}) \cdot (C_{p3}T_3 - C_{p4}T_4)} \quad (2)$$

$\dot{m}_{air}$ is the air mass flow rate through the compressor, kg/s; $\dot{m}_{hydrogen}$ is the hydrogen mass flow rate,

kg/s; C_{p1} is the specific heat capacity of the airflow before the compressor, kJ/kg·K; C_{p2} is the specific heat capacity of the airflow after the compressor, kJ/kg·K; T_1 is the temperature of the airflow before the compressor, K; T_2 is the temperature of the airflow after the compressor, K; C_{p3} is the specific heat capacity of the airflow before the turbine, kJ/kg·K; C_{p4} is the specific heat capacity of the airflow after the turbine, kJ/kg·K; T_3 is the temperature of the airflow before the turbine, K; T_4 is the temperature of the airflow after the turbine, K.

2.2 Matched VGT turbocharger

The hydrogen engine requires a well-matched turbocharger which depends on the desired performance at low speeds and high speeds. Variable geometry turbines are much more suited for turbocharged hydrogen engines across the whole operating map compared with waste gate turbochargers according to Lai et al.. The reduced air mass flow rates at 2500 rpm and 4500 rpm when the hydrogen engine operates at high loads are calculated according to the method in [41]. A BorgWarner VGT turbocharger where the mass flow rate varies from 0.00411(kg/s)·K^0.5/kPa to 0.02006(kg/s)·K^0.5/kPa was chosen for this work. As Figure 2 (a) shows, the calculated reduced mass flow rates match the operating range of the VGT turbocharger. In addition, the maximum air flow rate of the compressor reaches around 633 kg/h according to Figure 2 (b) which is sufficient for a 2.0 L hydrogen engine, and the shape of VGT is shown in Figure 2 (c).

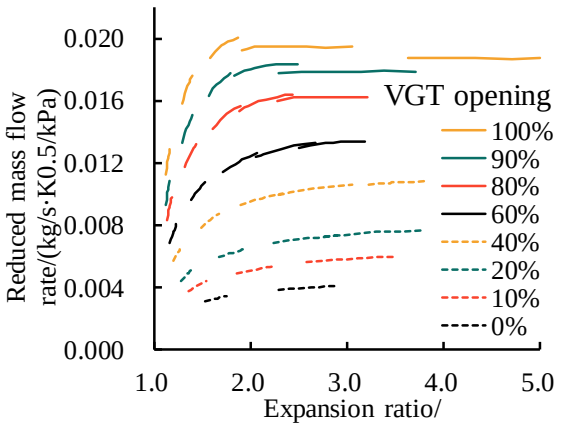

a) The BorgWarner VGT turbocharger operating

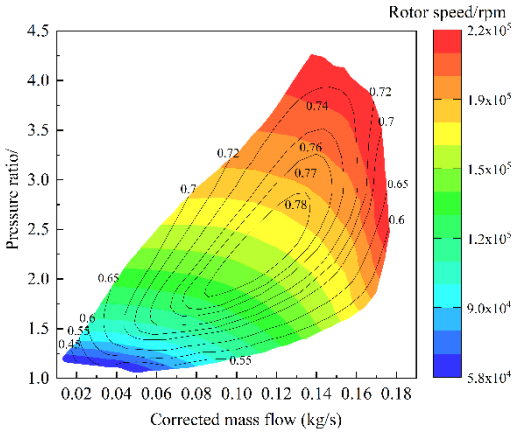

b) The compressor map of the VGT

range and calculated reduced mass flow rates turbocharger

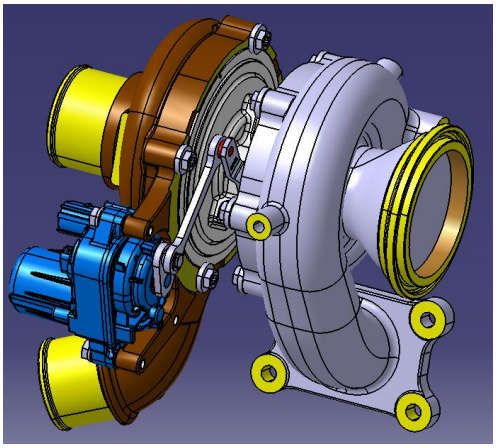

c) The model of BorgWarner VGT turbocharger

Figure 2 The details of the VGT turbocharger

3. Results and discussion

3.1 Boundary matching the VGT for a hydrogen engine

Considering the large flammability range and low ignition energy of hydrogen, a relatively rich mixture and high residual gas fraction may cause severe abnormal combustion. Thus, there exist operating limits in hydrogen engines that can be affected by VGT. The effect of VGT opening on λ and the exhaust back pressure factors are studied.

3.1.1 Upper limit boundary of VGT limited by λ due to abnormal combustion

Typical abnormal combustion affected by VGT matching in a hydrogen engine is depicted in Figure 3 (a). A severe knocking cycle is detected with a maximum cylinder pressure of 17 MPa at λ=1.61 with the VGT open to 35% at an engine speed of 1500 rpm. However, as shown in Figure 3 (b), since the combustion happens earlier than spark timing, it is more likely that pre-ignition occurs rather than knock at high loads [42]. At large VGT openings of 100% with λ=1.67 ultra-high peak pressures are observed with the potential to severely damage the engine. The research of Meske et al. [12] also reported that hydrogen's chemical properties make hydrogen engines particularly vulnerable to pre-ignition.

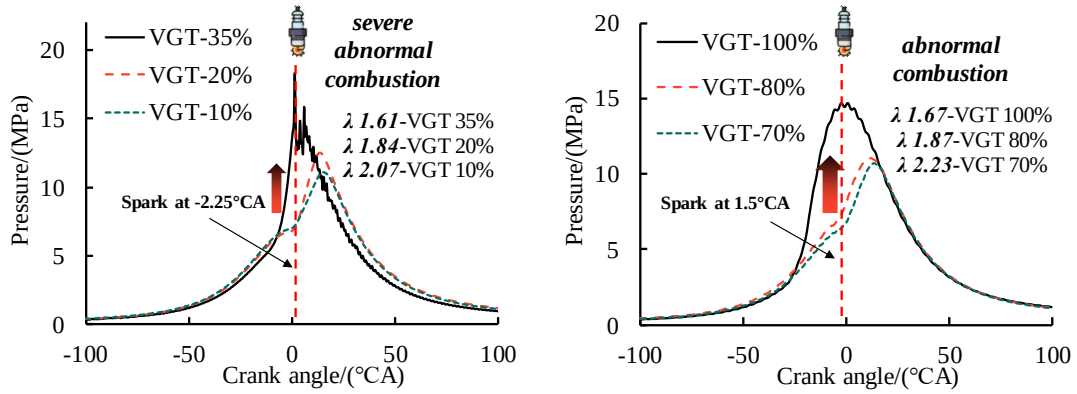

a) 1500rpm b) 4000rpm

Figure 3 The abnormal combustion occurs at different speeds and VGT openings

Figure 4 (a) shows that the maximum combustion temperature of the cylinder rises from 1255 K to 1549 K with increasing VGT opening. The tendency of the end-gases grows with an increasing VGT and the λ. In addition, the cooling losses climb from 26.7% to 31.7% which significantly affects the BTE, moving from 38.5% to 40%. Thus, λ variation needs to be evaluated in the VGT opening strategy. Secondly, abnormal combustion occurs frequently at some conditions which affects the hydrogen engine stability and the abnormal combustion is closely correlated to λ. The λ boundary with slight abnormal combustion is displayed in Figure 4 (b), and the engine power is restricted by the VGT opening boundary which corresponds to different λ. The minimum λ without abnormal combustion decreases from 1.53 to 1.35 as VGT opening increases from 50% to 80%. VGT opening at various engine speeds needs to be adjusted below the boundary to avoid abnormal combustion. Therefore, λ is one of the most important factors that should be considered in VGT opening optimization to avoid abnormal combustion.

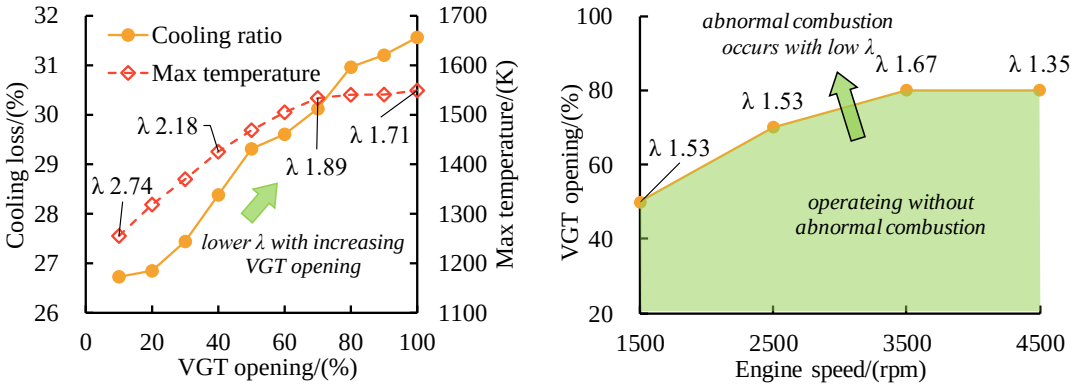

a) Cooling loss and max combustion temperature at different VGT openings

b) λ - abnormal combustion boundary at different speeds and VGT openings

Figure 4 Combustion parameters at 2000 rpm and λ boundary without abnormal combustion

3.1.2 Lower limit boundary of VGT limited by high exhaust back pressure

The impact of different VGT opening angles on the intake process is shown in Figure 5 (a) when the BMEP varies from 0.852 MPa to 0.898 MPa with a constant hydrogen flow rate of 2.24 kg/h at an engine speed of 2000 rpm. The intake pressure decreases from 0.179 MPa to 0.113 MPa and the exhaust back pressure decreases from 0.201 MPa to 0.114 MPa with increasing VGT opening from 10% to 100%. The difference between the exhaust back pressure and the intake pressure reduces with increased opening degree, and the intake pressure passes the exhaust back pressure gradually. A parameter of pumping mean effective pressure divided by indicated mean effective pressure (PMEP/IMEP) is used to evaluate the efficiency loss in the intake stroke. It reduces sharply from 5.4% to 2.43% with the VGT opening increasing from 10% to 30% and remains stable after the intake pressure exceeds the back pressure. In addition, high back pressure also leads to increased residual gases, rising unburned hydrogen emissions, and the occasional fire in the exhaust pipe with 0% VGT opening. The pumping loss can be observed in the P-V diagram in Figure 6 (b) at different VGT openings. The cylinder pressure in the intake stroke increases gradually due to the higher intake pressure. It is found that the shaded area of the pumping loss enclosed by the curve of the intake and

exhaust stroke reduces with the increasing VGT opening.

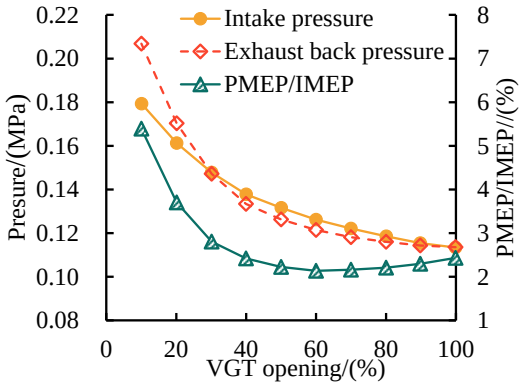

a) Pressure and PMEP/IMEP at 2000 rpm with different VGT openings

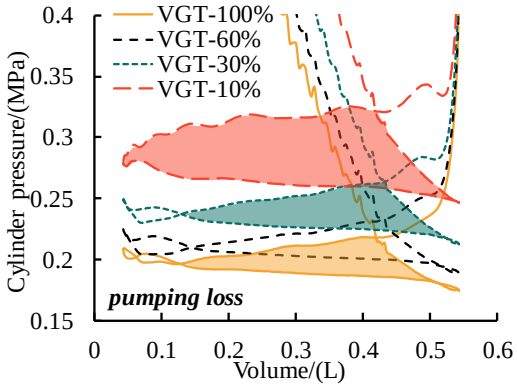

b) P-V diagram at 2000 rpm and different VGT openings

Figure 5 Variations of pumping loss and thermal efficiency at different VGT openings

As shown in Figure 6, exhaust back pressure affects the BTE and the TE differently. The BTE first increases from 38.72% to 40.06% and then drops sharply to 38.52% with increasing VGT opening when the intake valve opening (IVO) and exhaust valve closing (EVC) are set at -15°CA (negative values represent crank angles BTDC) and -10°CA respectively. The TE decreases from 55.7% to 37.8% constantly with a reduced backpressure from 206.8kPa to 113.5kPa. When the VGT changes from 0% to 30%, a faster burn duration of 24.0°CA to 19.7°CA is achieved. However, further turbo losses and heat transfer limit the improvement of BTE with a larger VGT opening. Thus, the optimum VGT opening is located between 30% to 40% with a lean λ cluster between 2.2 to 2.4.

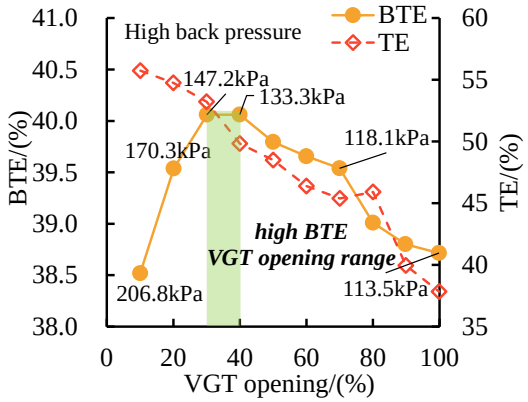

Figure 6 The BTE and TE variations at different VGT openings at the engine speed of 2000 rpm

The lower limit of VGT opening is determined in Figure 7 when the exhaust back pressure exceeds the intake pressure, and climbs from 10% to 40% as the engine speed changes from 1500 rpm to 4500 rpm. Exhaust back pressure exceeds 200kPa with low BMEP at different speeds when VGT opening is set at the boundary, and further reduction of VGT opening leads to higher pumping losses. The green shaded area illustrates the working boundary of the VGT limited by the abnormal combustion and high back pressure across the whole operating map.

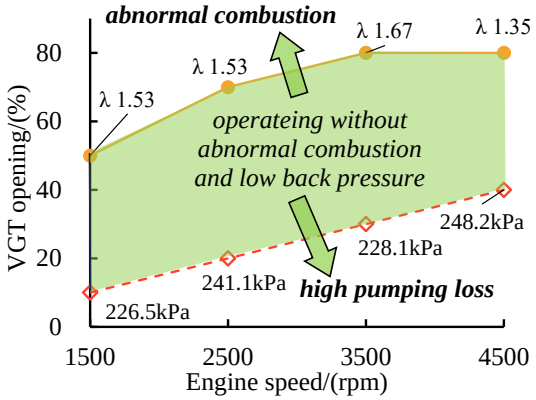

Figure 7 The boundary of VGT openings at different engine speeds

3.2 Optimizing control of the VGT with various targets

The working range of the VGT turbocharger still covers a large range after the boundary is determined and needs further optimization. Considering the optimal efficiency and power located at different operating conditions, separate strategies are proposed and compared as follows.

3.2.1 High-thermal efficiency optimization

According to previous studies, it is essential to evaluate the effect of both combustion and gas exchange processes to achieve higher BTE. Several tests of the operating conditions at a BMEP of 1.2 MPa have been conducted at an engine speed of 2500 rpm with the highest mechanical efficiency of approximately 86%. As depicted in Figure 7 (a), the BTE rises from 40.72% to 41.23% when VGT opening increases from 30% to

40%, and then it drops to 42.19% with 50% VGT opening. λ decreases from 2.53 to 2.04 and the pumping loss parameter PMEP/IMEP reduces from 2.60% to 1.25% with increasing VGT opening. In terms of the combustion parameters, the burn duration (BD) reduces from 23.8°CA to 19.7°CA with the decreasing λ according to Figure 7 (b), which improves the combustion efficiency. However, the cooling loss rises constantly from 22.0% to 24.3% preventing the further improvement of the BTE. Thus, a maximum BTE is achieved at 40% VGT opening by considering both the trade-off effects of pumping loss and proper combustion.

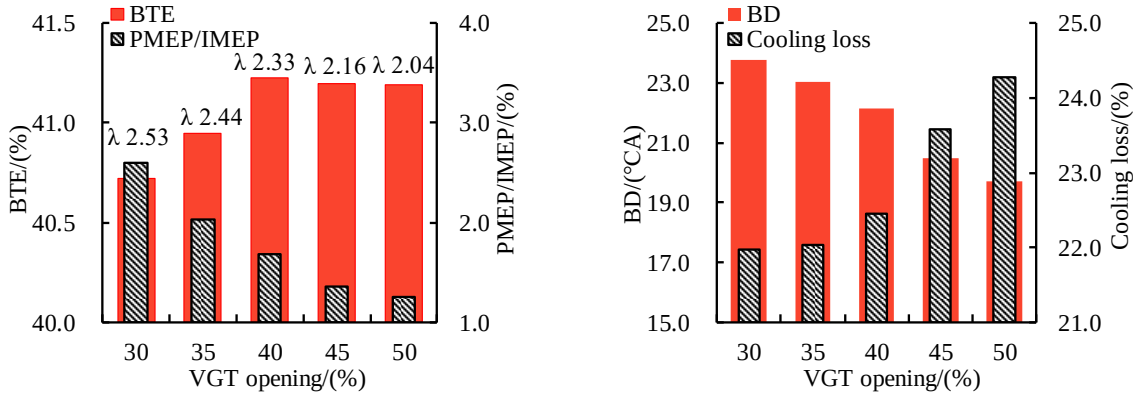

a) Variation of BTE and pumping loss

b) Variation in burn duration and cooling loss

Figure 7 The variation of performance and combustion parameters at 2500rpm at 1.2 MPa BMEP

A higher load is further investigated at an engine speed of 2500rpm to achieve the highest BTE. As shown in Figure 8 (a), lean λ ranges from 1.88 to 2.12 are achieved at a BMEP of 1.55 MPa. BTE improves from 41.75% to a maximum of 42.57% and then falls to 41.90% when VGT opening increases from 30% to 50%. Furthermore, cooling losses climb steadily from 21.5% to 22.8%, and PMEP/IMEP decreases from 2% to 1.2%. Optimal VGT opening is also located at 40% combining the two effects. According to the cylinder pressure in Figure 8 (b), the maximum pressure rises from 12.3 MPa to 13.9 MPa with decreased VGT opening from 50% to 30%, and the BD drops from 20.3°CA to 18.1°CA.

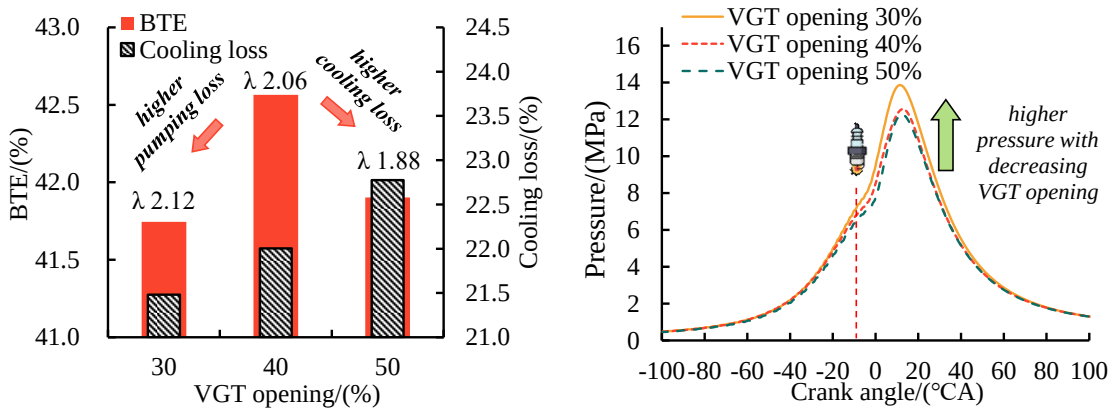

a) BTE and cooling loss

b) Cylinder pressure

Figure 8 Parameter variation at 2500 rpm with 1.55 MPa of BMEP

3.2.2 High-power optimization

When the hydrogen engine operates at high loads, a large airflow of over 300 kg/h is required to improve the power density and prevent abnormal combustion caused by low λ. Two methods of reducing VGT opening angle and adjusting VVT settings are effective in enhancing the air flow rate and tests are used to evaluate the best control strategy. The tests are conducted at 2500 rpm when the BMEP rises from 1.2 MPa to 1.23 MPa with an increase of λ from 2.05 to 2.5 to optimize the intake quality. As shown in Figure 9 (a), when the air flow increases from 260 kg/h to 319 kg/h, PMEP/IMEP increases from 1.6% to 4.8% while retarding EVC from 20°CA BTDC to 10°CA ATDC with a constant VGT opening of 50%. However, the PMEP/IMEP only rises from 1.3% to 2.6% when reducing VGT opening which is much lower than the earlier tests. As Figure 9 (b) displays, when it comes to the volumetric efficiency, this increases from 0.897 to 0.996 by adjusting VVT. However, the volumetric efficiency of the VGT strategy only increases from 0.870 to 0.888 and falls to 0.868 with a low VGT opening of 30% when the air flow rate is 319 kg/h. Therefore, changing VVT can optimize the intake process and lessen residual gas in the cylinders effectively, which helps cool the cylinder and prevent abnormal combustion. Reducing VGT opening angle exerts a positive impact on the pumping loss and the thermal efficiency. Therefore, reducing VGT is effective at medium loads with the BMEP below

1.7 MPa to retain high BTE; while adjusting VVT is necessary and is a priority when pursuing high power when the BMEP exceeds 1.7MPa at 2500rpm.

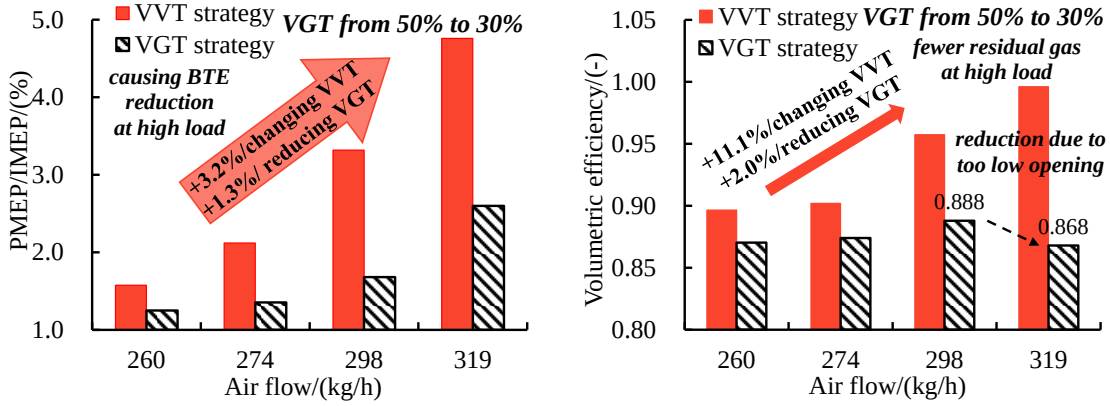

a) The PMEP/IMEP of two methods at different air flow rates

b) The volumetric efficiency of two methods at different air flow rates

Figure 9 Comparison of the two strategies at 2500 rpm with 1.2MPa to 1.23MPa of BMEP

Tests with different VGT openings are conducted at considerably higher loads of BMEP=1.82 MPa to expand the power limits. The results of 40% and 50% VGT opening are compared in Table 3. It can be found that λ drops from 2.11 to 1.99. Besides, PMEP/IMEP decreases from 5.4% to 5.0% and volumetric efficiency falls from 0.958 to 0.946. It is worth illustrating that the volumetric efficiency with 50% VGT opening drops because of an increase in intake temperature by 8℃ after the intercooler. The hydrogen engine operates stably at high loads since λ exceeds 1.99 with proper matching of the turbocharger. In addition, the exhaust temperature before the turbine increases from 525.5℃ to 536.4℃ when VGT opening climbs from 40% to 50%, which is beneficial to for the turbocharger to recover exhaust energy.

Table 3 The comparison of different VGT openings at 2500rpm with considerably high power

BMEP (MPa)	Power(kW)	VGT opening (%)	λ (/)	PMEP/IMEP (%)	Volumetric efficiency (/)	Exhaust temperature before turbine (℃)
1.82	75.7	40	2.11	5.4	0.958	525.5

1.81	75.3	50	1.99	5.0	0.946	536.4

However, λ reaches 1.66 at 1.62MPa BMEP at high engine speeds of 4500rpm with a 70% VGT opening according to Table 4. Further increasing the VGT opening to 80% leads to the PMEP/IMEP decrease from 8.3% to 7.3%, while λ drops to 1.36 and volumetric efficiency falls dramatically from 0.806 to 0.738. In addition, the λ of 1.36 approaches the abnormal combustion boundary of 80% VGT opening at 4500 rpm. Finally, maximum output power is enhanced from 121.3 kW with 70% VGT opening to 124.2 kW with 80% VGT opening. The high-power performance could be improved further with other methods such as enhancing wall cooling and promoting the hydrogen-air mixing to avoid locally rich gas mixtures. As for the exhaust temperature before the turbine, this increases from 660.6℃ to 746.0℃ when VGT opening climbs from 70% to 80%. Although the higher exhaust temperature provides more turbocharging capacity, the λ and volumetric efficiency suggest the hydrogen engine does not require a further larger VGT opening to achieve its maximum output power at 4500rpm.

Table 4 The comparison of different VGT openings at 4500rpm with considerably high loads

BMEP (MPa)	Power(kW)	VGT opening (%)	λ (/)	PMEP/IMEP (%)	Volumetric efficiency (/)	Exhaust temperature before turbine (℃)
1.62	121.3	70	1.66	8.3	0.806	660.6
1.63	124.2	80	1.36	7.3	0.738	746.0

3.3 The combined optimized strategy of VGT

Considering the above, the control strategy of the VGT should first obey the matching boundary limits and optimized strategies are separated when pursuing high BTE and power at different engine speeds. Here, an optimal VGT controlling strategy which is divided into five phases with different targets is proposed. The

definition of different phases is listed as follows:

Phase 1: At low loads, the VGT is opened wide to reduce pumping losses.

Phase 2: VGT opening decreases gradually and λ remains between 2.2 to 2.4, and BTE stays at high levels at the medium-low loads of the hydrogen engine.

Phase 3: VGT opening is set appropriately to maintain the balance between pumping loss and the λ effect on BTE to achieve higher performance.

Phase 4: At high loads, the VGT opening stays constant. The air flow rate needs to be enhanced to pursue high power, and VVT settings are optimized preferentially.

Phase 5: At very high loads, VGT opening attempts to increase to decrease pumping loss and expand the peak-power performance with no abnormal combustion.

Comparisons are also conducted with strategy I (pursuing high intake pressure with the lower limits of the VGT), strategy II (the optimal), and strategy III (pursuing minimal pumping loss with the upper limits of the VGT) to demonstrate the advantages of the optimal strategy. The intake pressure and BTE of different strategies are shown in Figure 10, where the intake pressure of strategy I is higher than that of strategy II, which leads to an increased λ, and the intake pressure at medium loads remains above 0.2 MPa. On the other hand, the intake pressure of strategy II constantly rises with increasing BMEP and reaches close to the intake pressure of strategy I at high loads. Even though the BTE of the two strategies varies little at high loads, there are significant differences between them at low and medium loads. The BTE can be optimized at low and medium loads by up to 2% utilizing strategy II. The intake pressure of strategy III is below 0.15 MPa at 2500rpm and below 0.17MPa at 4500rpm. There is still some reduction compared with strategy II in BTE at medium loads due to the low intake pressure and λ. More importantly, low λ reaches the abnormal combustion limits and the output power is restricted.

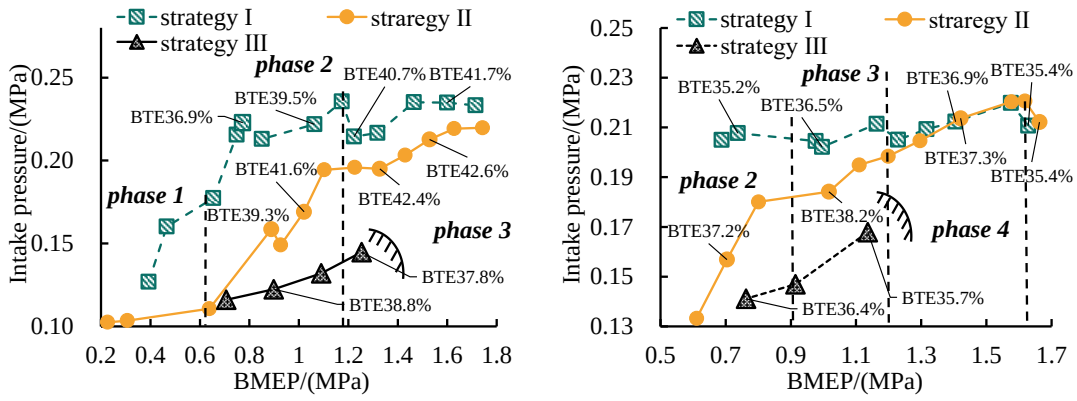

a) 2500 rpm b) 4500 rpm

Figure 10 The comparison of different VGT strategies on intake pressure and BTE

The operating states of different VGT opening strategies in compressor map and turbocharger efficiency are compared. Due to the low intake pressure, strategy III is not compared in the compressor map. According to Figure 11 (a), the airflow rates and pressure ratio of strategy II climb gradually with the rising BMEP at 2500rpm. On the other hand, the operating states of strategy I in the compressor map are mainly located with higher airflow while those of strategy II work with low-pressure ratio and compressor efficiency. When the BMEP increases, the difference between the two strategies on the compressor map narrows, and the compressor efficiency reaches above 78% when the BMEP increases to 1.7 MPa. The turbocharger efficiency is investigated further and the results are displayed in Figure 11 (b). As seen in Figure 11 (b), the TE of strategy II is at a full disadvantage when the hydrogen engine operates at low loads. The TE of strategy II achieves 23.3% and 30.9% when the BMEP attains 0.4 MPa and 0.77 MPa respectively, while that of strategy I reaches 38.7% and 49.0%. The variation of TE can be verified according to Figure 11 (a) - the gap of TE decreases as the BMEP increases constantly, and the TE of strategy I surpasses that of strategy II at 1.82 MPa despite the compressor efficiency of strategy II still being at a high level. Combined with the variation of the BTE, the VGT openings of strategy I still can be optimized further.

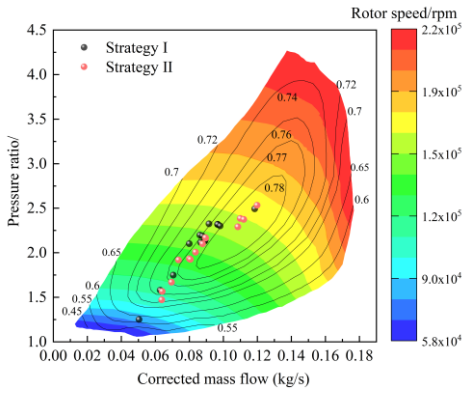

a) Operating states of different VGT opening strategies in the compressor map

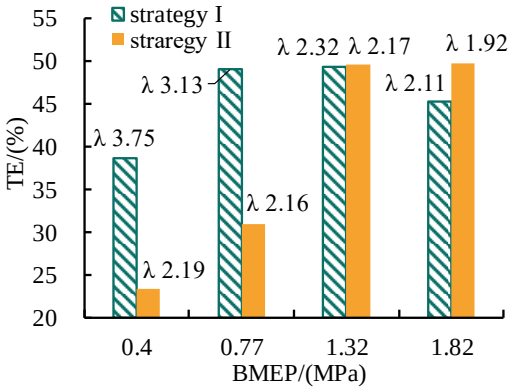

b) Turbocharger efficiency of different VGT opening strategies

Figure 11 Operating states of different VGT opening strategies and turbocharger efficiency

The λ variation of different phases at 2500rpm with different VGT strategies are displayed in Figure 12 (a). It can be observed the λ of strategy I which aims for greater turbocharging capacity, differs considerably from that of strategy II, particularly in phases 1 and 2. As the BMEP increases from 0.46 MPa to 1.22 MPa, the λ of strategy I reduces from 3.75 to 2.43 while that of strategy II mostly fluctuates between 2.2 to 2.4 at 2500 rpm. The λ gap between the two strategies becomes narrow with the rising BMEP. However, the λ of strategy III reduces from 2.32 to 1.63 when the BMEP climbs from 0.7 MPa to 1.25 MPa, and this low λ will lead to abnormal combustion. Figure 12 (b) shows the NOx variation at 2500rpm. The strategy III NOx emissions are generally higher than others at medium loads. The results show the NOx emissions of strategy I and II gradually increase after phase 2 with changing λ. At the maximum BMEP, the maximum NOx emission of strategy II reaches 547 ppm.

The BTE variation of different loads at 2500rpm and 4500rpm with different VGT strategies are displayed in Figure 12 (c) and (d). At 2500rpm, it can be observed the BTE variation reveals that strategy II is better than the others, and the maximum BTE reaches 42.57% and 38.35% at 2500 rpm and 4500 rpm respectively. Although the BTE of strategy I which aims for greater turbocharging capacity, is close to that

of strategy II at 2500 rpm at medium and high loads; and the superiority of strategy II is displayed more obviously at 4500rpm. In conclusion, strategy II is suggested as the optimum according to the intake pressure, λ, pumping loss, and TE at different loads. Finally, the VGT opening strategy II across the whole operating map from 1000 rpm to 4500 rpm is presented in Figure 12 (e). It can be found that the VGT opening remains 100% at each engine speed when the BMEP is below 0.4 MPa. At 2500rpm and 4500rpm, as the BMEP increases, the VGT opening gradually reduces to 40% and 75% respectively, and remains constant. When the high power is required, the VGT opening increases to 50% @ 2500rpm and 80% @ 4500rpm. Figure 12 (f) displays the λ variation across the whole operating map and it indicates a wide range of high efficiency (over 40%). A maximum torque of 326. 6 Nm at 2500rpm and a maximum power of 124.2 kW at 4500 rpm with a highest BTE of 42.57% are achieved. In addition, the torque at 1500 rpm reaches 322.3 Nm, which indicates the turbocharging is well matched at low and high speeds. This optimal strategy will be helpful in the development of hydrogen engine turbocharging.

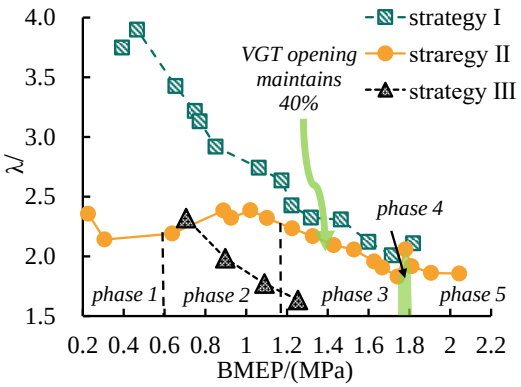

a) Whole operating map λ variation at 2500 rpm

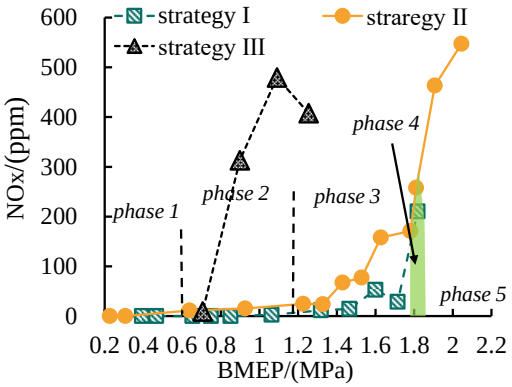

b) Whole operating map NOx variation at 2500 rpm

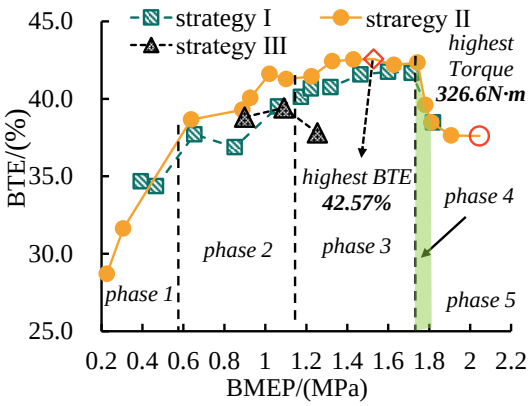

c) Whole operating map BTE variation at 2500 rpm

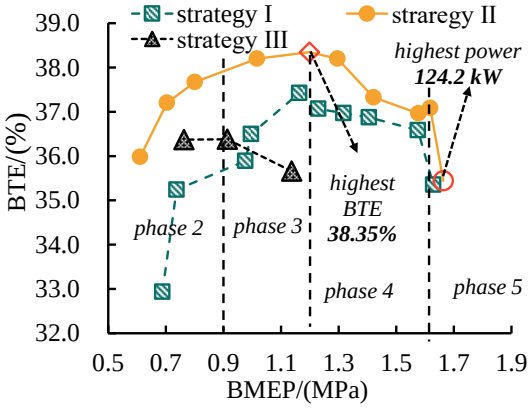

d) Whole operating map BTE variation at 4500 rpm

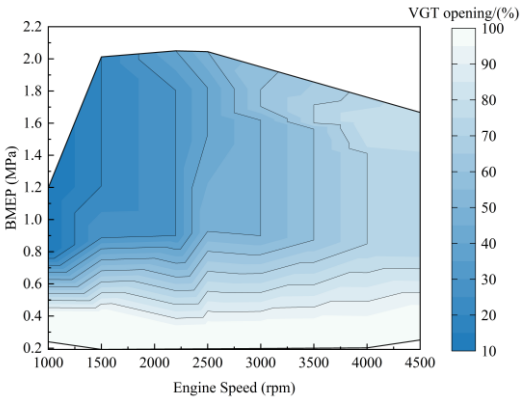

e) Whole operating map VGT opening strategy

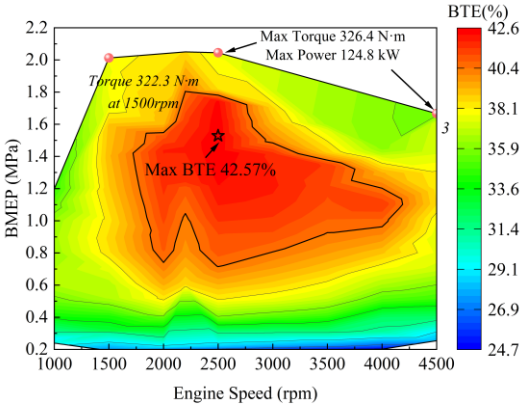

f) Whole operating map BTE variation

Figure 12 λ and BTE variation of different phases and the optimized VGT opening strategy across the Whole operating map

Conclusion

This research investigates experiments on a turbocharged direct-injected hydrogen engine with a VGT turbocharger, and the VGT opening control at different loads is studied. The following conclusions are drawn from the test results:

1. Since the high air-fuel ratio and air flow rate requirements of hydrogen engines, high back pressure with high pumping losses is the main factor in VGT opening optimization to achieve high thermal efficiency. λ is

another main factor in VGT opening optimization according to variation of BTE and abnormal combustion limits at different VGT openings. Two factors generate VGT opening lower and upper limits as the VGT opening boundary changes from 10%-50% at 1500 rpm to 40%-75% at 4500 rpm.

2. An optimal VGT opening strategy to balance the effects of pumping loss and λ is proposed. The results show the VGT opening optimization is a trade-off between pumping loss and cooling losses which both affect the BTE.

3. The maximum BTE can be reached by optimizing VGT opening with a λ between 2.2 to 2.4 at medium loads. In addition, the combination control of VVT and VGT opening is studied. It indicates VVT settings should be changed preferentially due to higher volumetric efficiency when the hydrogen engine operates at medium-high loads as more airflow is required to maintain the power and the VGT opening stays the same constantly.

4. The hydrogen engine optimized VGT opening control strategy is proposed, and it is divided into five phases according to λ control at different loads. In the first two phases, VGT opening gradually reduces from 100% to keep λ between 2.2 to 2.4 to improve BTE. For the next phase, the effects of pumping loss and λ are taken into consideration to achieve high efficiency, and the VGT opening remains constant. As for the last two phases which are for high power, VGT opening keeps constant when the VVT settings are changed preferentially to increase λ as the engine load climbs. Following that, VGT opening increases to reduce pumping losses, as well as λ, and expand the high-power performance without abnormal combustion.

5. A maximum torque of 326.6 Nm at 2500 rpm and a maximum power of 124.2 kW at 4500 rpm with the highest BTE of 42.57% are attained in the 2.0 L DI hydrogen engine. In addition, a torque of 322.3 Nm at 1500 rpm is achieved which is respectable at low speeds. The VGT opening control strategy based on λ and BTE can be valuable in the development of hydrogen engine turbocharging.

Reference

[1] Liu K, Pei Z, Yang H, Yang J, Li Y, Feng X. Investigation of the control strategy for hydrogen addition in all operating conditions of a high compression ratio liquid methane heavy-duty engine. Fuel 2024;359:130437. https://doi.org/10.1016/j.fuel.2023.130437.

[2] Le TT, Sharma P, Bora BJ, Tran VD, Truong TH, Le HC, et al. Fueling the future: A comprehensive review of hydrogen energy systems and their challenges. International Journal of Hydrogen Energy 2023:S0360319923039988. https://doi.org/10.1016/j.ijhydene.2023.08.044.

[3] Teoh YH, How HG, Le TD, Nguyen HT, Loo DL, Rashid T, et al. A review on production and implementation of hydrogen as a green fuel in internal combustion engines. Fuel 2023;333:126525. https://doi.org/10.1016/j.fuel.2022.126525.

[4] Kurien C, Mittal M. Utilization of green ammonia as a hydrogen energy carrier for decarbonization in spark ignition engines. International Journal of Hydrogen Energy 2023;48:28803–23. https://doi.org/10.1016/j.ijhydene.2023.04.073.

[5] Kurien C, Mittal M. Review on the production and utilization of green ammonia as an alternate fuel in dual-fuel compression ignition engines. Energy Conversion and Management 2022;251:114990. https://doi.org/10.1016/j.enconman.2021.114990.

[6] Wang B, Wang H, Yang C, Hu D, Duan B, Wang Y. Effect of different ammonia/methanol ratios on engine combustion and emission performance. Applied Thermal Engineering 2024;236:121519. https://doi.org/10.1016/j.applthermaleng.2023.121519.

[7] Tian Z, Wang Y, Zhen X, Liu Z. The effect of methanol production and application in internal combustion engines on emissions in the context of carbon neutrality: A review. Fuel 2022;320:123902.

https://doi.org/10.1016/j.fuel.2022.123902.

[8] Seboldt D, Mansbart M, Grabner P, Eichlseder H. Hydrogen Engines for Future Passenger Cars and Light Commercial Vehicles. MTZ Worldw 2021;82:42–7. https://doi.org/10.1007/s38313-020-0603-1.

[9] Barış O, Güler İ, Yaşgül A. The effect of different charging concepts on hydrogen fuelled internal combustion engines. Fuel 2023;343:127983. https://doi.org/10.1016/j.fuel.2023.127983.

[10] Hong C, Ji C, Wang S, Xin G, Qiang Y, Yang J. Progressive strategies to avoid and exploit knock limit for optimal performance and stoichiometric operation of a DI hydrogen engine with high CR at WOT conditions. Fuel 2024;357:129849. https://doi.org/10.1016/j.fuel.2023.129849.

[11] Chaudhary K, Bhardvaj K, Chaudhary A. A qualitative assessment of hydrogen generation techniques for fuel cell applications. Fuel 2024;358:130090. https://doi.org/10.1016/j.fuel.2023.130090.

[12] Meske, P., Schmidt, K., Shiba, H., Capellmann, D. et al. Component and Combustion Optimization of a Hydrogen Internal Combustion Engine to Reach High Specific Power for Heavy-Duty Applications. SAE Technical Paper 2023-01-0038, 2023. https://doi.org/10.4271/2023-32-0038.

[13] Verhelst S, Wallner T. Hydrogen-fueled internal combustion engines. Progress in Energy and Combustion Science 2009;35:490–527. https://doi.org/10.1016/j.pecs.2009.08.001.

[14] Dimitriou P, Tsujimura T. A review of hydrogen as a compression ignition engine fuel. International Journal of Hydrogen Energy 2017;42:24470–86. https://doi.org/10.1016/j.ijhydene.2017.07.232.

[15] Kalaskar, V., Conway, G., Handa, G., Joo, S. et al. Challenges and Opportunities with Direct-Injection Hydrogen Engines, SAE Technical Paper 2023-01-0287, 2023. https://doi.org/10.4271/2023-01-0287.

[16] Sterlepper S, Fischer M, Claßen J, Huth V, Pischinger S. Concepts for Hydrogen Internal Combustion Engines and Their Implications on the Exhaust Gas Aftertreatment System. Energies 2021;14:8166. https://doi.org/10.3390/en14238166.

[17] Natkin, R., Denlinger, A., Younkins, M., Weimer, A. et al. Ford 6.8L Hydrogen IC Engine for the E-450 Shuttle Van. SAE Technical Paper 2007-01-4096, 2007. https://doi.org/10.4271/2007-01-4096.

[18] Berckmüller, M., Rottengruber, H., Eder, A., Brehm, N. et al. Potentials of a Charged SI-Hydrogen Engine. SAE Technical Paper 2003-01-3210, 2003. https://doi.org/10.4271/2003-01-3210.

[19] Krishnanunni J, Bhatia D, Dutta V, Das LM. Power Improvement and NOx Reduction Strategies for a Hydrogen-Fueled Multicylinder Internal Combustion Engine. Journal of Engineering for Gas Turbines and Power 2019;141:121001. https://doi.org/10.1115/1.4044966.

[20] Bao L, Sun B, Luo Q, Li J, Qian D, Ma H, et al. Development of a turbocharged direct-injection hydrogen engine to achieve clean, efficient, and high-power performance. Fuel 2022;324:124713. https://doi.org/10.1016/j.fuel.2022.124713.

[21] Bao L, Sun B, Luo Q. Optimal control strategy of the turbocharged direct-injection hydrogen engine to achieve near-zero emissions with large power and high brake thermal efficiency. Fuel 2022;325:124913. https://doi.org/10.1016/j.fuel.2022.124913.

[22] Luo, Q. and Lee, C. Controlling Strategy for the Performance and NOx Emissions of the Hydrogen Internal Combustion Engines with a Turbocharger. SAE Technical Paper 2020-01-0256, 2020. https://doi.org/10.4271/2020-01-0256.

[23] Lee J, Park C, Kim Y, Choi Y, Bae J, Lim B. Effect of turbocharger on performance and thermal efficiency of hydrogen-fueled spark ignition engine. International Journal of Hydrogen Energy 2019;44:4350–60. https://doi.org/10.1016/j.ijhydene.2018.12.113.

[24] Jilakara S, Vaithianathan JV, Natarajan S, Ramakrishnan VR, Subash G, Abraham M, et al. An Experimental Study of Turbocharged Hydrogen Fuelled Internal Combustion Engine. SAE Int J Engines 2015;8:314–25. https://doi.org/10.4271/2015-26-0051.

[25] Nguyen D, Choi Y, Park C, Kim Y, Lee J. Effect of supercharger system on power enhancement of hydrogen-fueled spark-ignition engine under low-load condition. International Journal of Hydrogen Energy 2021;46:6928–36. https://doi.org/10.1016/j.ijhydene.2020.11.144.

[26] Dahham, R.Y.; Wei, H.; Pan, J. Improving Thermal Efficiency of Internal Combustion Engines: Recent Progress and Remaining Challenges. Energies 2022, 15, 6222, doi:10.3390/en15176222.

[27] Wang J, Shen L, Bi Y, Lei J. Influences of a variable nozzle turbocharger on the combustion and emissions of a light-duty diesel engine at different altitudes. Fuel 2023;349:128626. https://doi.org/10.1016/j.fuel.2023.128626.

[28] Tang H, Pennycott A, Akehurst S, Brace CJ. A review of the application of variable geometry turbines to the downsized gasoline engine. International Journal of Engine Research 2015;16:810–25. https://doi.org/10.1177/1468087414552289.

[29] Llamas X, Eriksson L. Optimal Transient Control of a Heavy Duty Diesel Engine with EGR and VGT. IFAC Proceedings Volumes 2014;47:11854–9. https://doi.org/10.3182/20140824-6-ZA-1003.01520.

[30] Galindo J, Serrano JR, De La Morena J, Gómez-Vilanova A. Physical-based variable geometry turbines predictive control to enhance new hybrid powertrains' transient response. Energy 2022;261:125189. https://doi.org/10.1016/j.energy.2022.125189.

[31] Feneley AJ, Pesiridis A, Andwari AM. Variable Geometry Turbocharger Technologies for Exhaust Energy Recovery and Boosting-A Review. Renewable and Sustainable Energy Reviews 2017;71:959–75. https://doi.org/10.1016/j.rser.2016.12.125.

[32] Jinnai Y, Arimizu H, Tashiro N, Tojo M, Yokoyama T, Hayashi N. A Variable Geometry (VG) Turbocharger for Passenger Cars to Meet European Union Emission Regulations 2012;49.

[33] Feneley AJ, Pesiridis A, Andwari AM. Variable Geometry Turbocharger Technologies for Exhaust

Energy Recovery and Boosting-A Review. Renewable and Sustainable Energy Reviews 2017;71:959–75. https://doi.org/10.1016/j.rser.2016.12.125.

[34] Kim J, Rajoo S. A Numerical Study on Turbocharging System for PFI-SI Type Hydrogen Combustion Engine. SAE Technical Paper 2021-24–0094, 2021. https://doi.org/10.4271/2021-24-0094.

[35] Hiyama D, Ito A, Nishibe K, Nozaki S, Nanba Y, Yamaura T, et al. A Study on Developing MPI Hydrogen ICE over 2MPa BMEP for Medium Duty Vehicles. SAE Technical Paper 2023-32–0037, 2023. https://doi.org/10.4271/2023-32-0037.

[36] Brin J, Waldron T. Analysis of Boosting Architectures for Hydrogen Internal Combustion Engines. SAE Technical Paper 2023-01–0411, 2023. https://doi.org/10.4271/2023-01-0411.

[37] Kim J, Rajoo S. A Numerical Study on Turbocharging System for PFI-SI Type Hydrogen Combustion Engine, 2021, p. 2021-24–0094. https://doi.org/10.4271/2021-24-0094.

[38] Barış O, Güler İ, Yaşgül A. The effect of different charging concepts on hydrogen fuelled internal combustion engines. Fuel 2023;343:127983. https://doi.org/10.1016/j.fuel.2023.127983.

[39] Kim C, Park C, Kim Y, Choi Y. Power characteristics with different types of turbochargers for lean boosted hydrogen direct injection engine in NOx-free operation. Heliyon 2023;9:e14186. https://doi.org/10.1016/j.heliyon.2023.e14186.

[40] Gürbüz H, Akçay İH, Buran D. An investigation on effect of in-cylinder swirl flow on performance, combustion and cyclic variations in hydrogen fuelled spark ignition engine. Journal of the Energy Institute 2014;87:1–10. https://doi.org/10.1016/j.joei.2012.03.001.

[41] Lai F, Sun B, Xiao G, Luo Q, Bao L. Research on optimizing turbo-matching of a large-displacement PFI hydrogen engine to achieve high-power performance. International Journal of Hydrogen Energy 2023;48:38508–20. https://doi.org/10.1016/j.ijhydene.2023.06.104.

[42] Wang K, Zhang Z, Sun B, Zhang S, Lai F, Ma N, et al. Experimental investigation of the working boundary limited by abnormal combustion and the combustion characteristics of a turbocharged direct injection hydrogen engine. Energy Conversion and Management 2024;299:117861. https://doi.org/10.1016/j.enconman.2023.117861.